Renewable and Sustainable Energy Reviews 161 (2022) 112302

Contents lists available at ScienceDirect

Renewable and Sustainable Energy Reviews

journal homepage: www.elsevier.com/locate/rser

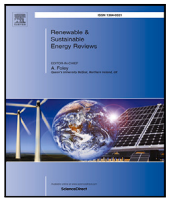

Spectral integration of clear-sky atmospheric transmittance: Review and worldwide performance

José A. Ruiz-Arias *

Applied Physics I, University of Málaga, Málaga, Spain
Solargis s.r.o., Bratislava, Slovakia

ARTICLE INFO

Keywords:
Broadband atmospheric transmittance
Spectral integration
Worldwide evaluation error
Clear-sky solar radiation

ABSTRACT

Broadband atmospheric transmittance is a key component in many broadband clear-sky solar radiation models, whose performance is inevitably bound to the goodness of their atmospheric transmittance parameterizations. A key element in the development of these parameterizations, that has been traditionally overlooked, is the spectral integration to the broadband range. The related scientific literature reveals that two different spectral integration approaches have been proposed, but they have been vaguely evaluated despite the central role of broadband transmittance. This work discusses such approaches, proposes new ones that mitigate current issues and conducts an unprecedented worldwide evaluation study that analyzes the direct normal irradiance evaluation error that is directly attributable to the choice of spectral integration approach. The study makes use of more than 7 million atmospheric transmittance spectra and a 1-year hourly simulation across a 2-degree spatial grid worldwide. The results show that the independent integration scheme, which is the one virtually used always, results in deviations as high as ±40 W/m^2 in dry and clean, and in humid and turbid environmental conditions. Overall, while the error stays within ±20 W/m^2 for 90% of the cases worldwide using the independent scheme, it is reduced to only ±1.5 W/m^2 using one of the alternative integration schemes here proposed. Hence, as a matter of conclusion, it is recommended that any broadband clear-sky solar irradiance model intended for global applications considers a higher-performance spectral integration scheme for atmospheric transmittance, such as the ones proposed here.

1. Introduction

Broadband or wideband atmospheric transmittance is a key aspect in the radiative transfer of the atmosphere [1,2], as it is also in the realm of broadband clear-sky solar radiation models (hereinafter referred to as CSR models) [3–6]. In solar applications, the term *broadband* refers to the spectral range typically from 0.29 to 4 μm, and so, broadband transmittance has to be evaluated throughout this entire band. Broadband transmittance is just a convenient extension of monochromatic light's transmittance to the entire solar spectral range that prevents spectral computations during the calculation of broadband solar irradiance.

CSR models are routinely used in solar applications [7–19] and undergo regular benchmark exercises [20–27]. Their performance is constrained by that of the transmittance functions in which they rely on. Hence, it is of utmost importance to use high-performance functions to build atmospheric transmittance. The parameterization of broadband atmospheric transmittance as a custom transmittance function is a two-step process: (1) the *integration stage*, in which the spectral atmospheric transmittance is integrated throughout the broadband spectral range, and (2) the *parameterization stage*, in which the integrated transmittance is parameterized as a custom function of solar position and the atmospheric state. Both the integration stage and the parameterization stage result in errors that contribute to the solar irradiance computation error. However, while the parameterization errors are a frequent source of concern and review, the errors that emanate from the integration stage are very often overlooked. This work reviews the most common spectral integration approaches, propose variations of them with arguable benefits and validate all schemes worldwide.

The next section motivates the use of broadband transmittance functions in CSR models, with the focus on direct normal irradiance, as a first step to understand the various spectral integration schemes.

1.1. Modeling broadband direct normal irradiance

A photon that traverses the atmosphere is subjected to *extinction*, i.e., removal from its straight travel path, by interacting with the

* Correspondence to: Applied Physics I, University of Málaga, Málaga, Spain.
E-mail addresses: jararias@uma.es, jose.ruiz-arias@solargis.com.

https://doi.org/10.1016/j.rser.2022.112302
Received 21 December 2021; Received in revised form 13 February 2022; Accepted 19 February 2022
Available online 15 March 2022

multiple atmospheric constituents (e.g., air molecules, water vapor and aerosol particles). The fraction of photons that emerge in the same direction and with the same wavelength as they enter the atmosphere is known as transmittance and is evaluated separately for each atmospheric constituent, i, and photon's wavelength, λ. It is calculated in virtue of the Bouguer's law [28] as:

$$\tau_{i\lambda} = e^{-m_i \delta_{i\lambda}}, \tag{1}$$

where m_i and $\delta_{i\lambda}$ are the optical air mass and the optical thickness of the i-th atmosphere's constituent, respectively. Note that $\delta_{i\lambda}$ is a spectral quantity, thereby, transmittance is *fundamentally* a spectral magnitude.

Extinction is explained at fundamental level in terms of discrete interactions between monochromatic light and matter. In sparse media, such as the atmosphere, these interactions are independent each other [29]. An immediate consequence is that the monochromatic direct normal irradiance at the surface, $E_{bn\lambda}$, can be evaluated as the solar flux at the top of the atmosphere, $E_{0n\lambda}$, successively reduced by the extinctions due to every atmospheric constituent. Most often, five extinction processes are considered in a cloudless atmosphere (e.g., [3]):

$$E_{bn\lambda} = E_{0n\lambda}\ \tau_{o\lambda}\ \tau_{r\lambda}\ \tau_{g\lambda}\ \tau_{w\lambda}\ \tau_{a\lambda}, \tag{2}$$

where $\tau_{o\lambda}$ is the absorption transmittance by stratospheric and tropospheric ozone, $\tau_{r\lambda}$ is the transmittance by molecular (or Rayleigh) scattering, $\tau_{g\lambda}$ is the absorption transmittance by air molecules, $\tau_{w\lambda}$ is the absorption transmittance by water vapor and $\tau_{a\lambda}$ is the transmittance due to absorption and scattering by aerosols.

The broadband direct normal irradiance, E_{bn}, over the spectral range $\Delta\lambda$ is then calculated as:

$$E_{bn} = \int_{\Delta\lambda} E_{0n\lambda}\ \tau_{o\lambda}\ \tau_{r\lambda}\ \tau_{g\lambda}\ \tau_{w\lambda}\ \tau_{a\lambda}\ d\lambda. \tag{3}$$

When spectral details are not needed and only the broadband solar irradiance E_{bn} is of interest, which is a most usual case in solar applications, the spectral calculations involved in Eq. (3) are often circumvented using *broadband parameterizations* of the atmospheric transmittances. The most widely-used parameterization form, hereinafter referred to as $\hat{E}_{bn}$, *assumes* that the atmospheric extinction processes at the broadband level are independent, exactly as they are at monochromatic level. Hence, following similar principles to Eq. (2):

$$\hat{E}_{bn} = E_{0n}\ T_o\ T_r\ T_g\ T_w\ T_a, \tag{4}$$

where $E_{0n} = \int_{\Delta\lambda} E_{0n\lambda}\ d\lambda$ is the total extraterrestrial irradiance and T_i are the broadband transmittances due to every i-th atmospheric constituent in the spectral range $\Delta\lambda$ [30]. As $\hat{E}_{bn}$ approximates the true E_{bn}, the difference $\hat{E}_{bn} - E_{bn}$ is hereinafter referred to as E_{bn} *approximation error*.

Similarly, and in analogy with Eq. (1), T_i is sometimes parameterized as:

$$T_i = e^{-m_i \delta_i}, \tag{5}$$

where δ_i is the broadband twin of $\delta_{i\lambda}$.

At this point, it must be emphasized that Eqs. (4) and (5) are just *idealizations* without further justification beyond the analogy with their spectral counterparts. Furthermore, they condition the choice of spectral integration approach, as it will be discussed in Section 1.2.

1.2. Spectral integration schemes

If $\tau_{i\lambda}$ is known for every λ, the simplest approach to obtain its broadband counterpart T_i is the arithmetic average, i.e., $\int_{\Delta\lambda} \tau_{i\lambda}\ d\lambda / \int_{\Delta\lambda} d\lambda$. However, considering that the variation of $\tau_{i\lambda}$ within the interval $\Delta\lambda$ may not be negligible, the broadband transmittance is preferentially evaluated as a weighted average of $\tau_{i\lambda}$ with weighting function determined from the extraterrestrial spectral irradiance as follows:

$$T_i = \frac{\int_{\Delta\lambda} E_{0n\lambda}\ \tau_{i\lambda}\ d\lambda}{\int_{\Delta\lambda} E_{0n\lambda}\ d\lambda}. \tag{6}$$

Following the naming convention used by [31], Eq. (6) is hereafter referred to as *independent* (INDEP) integration scheme.

Although this approach is conceptually simple, it presents a fundamental flaw: Combined with $\hat{E}_{bn}$ in Eq. (4), it does not reduce to E_{bn}, resulting thus in a parameterization error, hereinafter referred to as INDEP *'s pitfall*. The only exception occurs when the spectral interval $\Delta\lambda$ is so narrow that the variation of $\tau_{i\lambda}$ is negligible for all atmospheric constituents. Hence, the INDEP scheme is suitable only for narrow spectral bands but may result in remarkable errors in wide bands, such as the broadband solar range.

Precisely the INDEP's pitfall led to the proposal of the next alternative definition [31]:

$$T_i = \frac{\int_{\Delta\lambda} E_{0n\lambda}\ \prod_{k=1}^{i} \tau_{k\lambda}\ d\lambda}{\int_{\Delta\lambda} E_{0n\lambda}\ \prod_{k=1}^{i-1} \tau_{k\lambda}\ d\lambda} \tag{7}$$

which reduces $\hat{E}_{bn}$ to Eq. (3), thus resulting in null E_{bn} approximation error. However, this definition is not free from other issues, as it will become clear in Section 1.3. Following the naming convention used by [31], Eq. (7) is hereinafter referred to as *interdependent* (INTER) integration scheme.

The INTER scheme relies on the conceptual (although unrealistic) idea that the atmosphere is arranged into disjoint layers along which every constituent distributes homogeneously, one per layer, with no mixing with each other. With this vertical arrangement of the atmosphere, the incoming solar irradiance at the top of any atmospheric layer has been already extinguished by the constituents in the layers above, which motivates the definition of the scheme as outlined in Eq. (7).

A formal flaw of the INTER scheme is that the definition of the individual broadband transmittances depends on the arrangement of layers in the atmosphere. If the ordering of such layers changes, it does so the definition of the individual broadband transmittances. Hence, although this fact does not affect the calculation of total transmittance, the INTER broadband transmittances must be interpreted with care when they are used to evaluate the impact by individual atmospheric constituents.

The interested reader may find further details in the pioneering works of [31–33].

1.3. Parameterization of integrated broadband transmittances

The broadband transmittances calculated with the INDEP and INTER integration schemes do not depend on the light's wavelength but only on the type and amount of atmospheric constituents. As a result, they can be parameterized, during the parameterization stage, as custom functions of solar position and parameters related to the atmospheric state (e.g., total-column water vapor content for water vapor absorption or aerosol optical depth for aerosol transmittance). However, the choice of spectral integration scheme has strong implications on the complexity of such parameterizations.

The INDEP scheme leads to relatively simple functional dependences that are straightforward to parameterize because the impact of the different atmospheric constituents on the broadband transmittances is fully isolated. Conversely, the INTER scheme involves secondary dependences that hinder the parameterization process as a function of air mass and the amount of atmospheric constituents. In particular, for instance, the broadband transmittance of the lowermost atmospheric layer in the INTER scheme depends on all the atmospheric constituents aloft, which creates complicated inter-relations between the constituents, air mass and transmittance that are difficult to parameterize. Thereby, it also results in likely parameterization errors during the

parameterization stage combined with complex and computationally-demanding calculations, which, overall, is hereinafter referred to as the INTER *'s pitfall*.

The related scientific literature reveals that the INDEP scheme is the preferred choice to accomplish the spectral integration of atmospheric transmittance [e.g.,1,4,30,33–48] despite only the INTER scheme guarantees exact E_{bn} parameterization in combination with Eq. (4). It means that the error by the INDEP's pitfall is neglected, or rather, the augmented parameterization complexity by the INTER's pitfall is deemed too high.

To the knowledge of this author, [4] is the only work that has addressed so far a true inter-comparison of the performance results obtained by direct solar transmittance parameterizations based on the INDEP and the INTER schemes. Not surprisingly, the *MultiLayer-Weighted Transmittance direct irradiance model, version 2* (MLWT2), whose broadband transmittances follow the INTER scheme, provided the best results in all tests. These results were at the expense of an increased complexity in the parameterization of the broadband transmittances that involved a computational burden about three times higher than that for the *Reference Evaluation of Solar Transmittance model* (REST). The REST model was also developed within the framework of that work, using similar numerical parameterizations than for MLWT2, but relying on the INDEP scheme. Considering that both MLWT2 and REST are models recommended by [4] because they predict direct irradiance within the uncertainty of well-maintained pyrheliometers, complexity seems to be the reason that has tipped the balance in favor of the INDEP scheme for broadband transmittance parameterizations.

A particularly interesting case that deserves attention is that of the REST2 model [49], because it is consistently ranked high in benchmark studies [8,23,25,26]. According to [49], the formalism to derive the REST2's wideband atmospheric transmittances is the same as in the CPCR2 model [35], where it is made clear that transmittances are derived using the INDEP approach. However, Dr. Gueymard confirmed in a personal communication that indeed the REST2 aerosol transmittance follow the INTER integration scheme and referred to [13] for further details on the parameterization process in REST2. In particular, he noted that aerosol transmittance in REST2 is parameterized from the *Simple Model of the Atmospheric Transfer of Sunshine v2* (SMARTS2) [3,50–52] as the ratio of direct normal irradiance obtained for the actual atmospheric Ångström's turbidity and exponent values to that for an atmosphere with no aerosols and fixed values for precipitable water, total columnar ozone content and atmospheric pressure. The fact that some of the atmospheric constituents are prescribed in the aerosol transmittance parameterization highlights the complexity increase that comes with the INTER scheme and the practical need to relax such complexity during the parameterization stage to make the parameterization task affordable.

In this context, this work quantifies the worldwide E_{bn} approximation error using Eq. (4) in combination with different spectral integration schemes of the atmospheric transmittance. Thus, the novelty of this study is that the focus is in the performance analysis of the *integration* stage, conversely to the typical case in which the focus is in the parameterization stage. The E_{bn} approximation error is evaluated using three variations of the INDEP and INTER schemes to integrate the spectral atmospheric transmittances: (i) a 2-band version of the INDEP scheme, which is being already used in existing models but has not been extensively validated so far; (ii) a variation of the INTER scheme using a prescribed clean atmosphere that prevents the INTER's pitfall; and (iii) a hybrid approach that combines the principles of the 2-band INDEP and prescribed INTER schemes. The performances of the INDEP, 2-band INDEP, prescribed INTER and hybrid spectral integration schemes are thoroughly analyzed in terms of the E_{bn} approximation error or, equivalently, the total transmittance error. The analysis is based on the calculated transmittance spectra for more than 1.4 million hypothetical atmospheres (involving the calculation of about 7 million transmittance spectra) and a 1-year hourly worldwide simulation across a 2-degree spatial grid.

Section 2 describes the modified versions of the INDEP and INTER integration schemes. Section 3 introduces the spectral models used to simulate the spectral transmittances for each atmospheric constituent and describes the generation of the broadband transmittance data bases which are subsequently analyzed in Section 4. The main conclusions are summarized in Section 5.

2. Alternative spectral integration schemes

2.1. 2-band independent integration scheme

The INDEP's pitfall vanishes with infinitesimally narrow spectral bands. However, it can be largely reduced too in the broadband solar range (0.29–4 μm) even with only two wisely selected bands. The absorption by water vapor and gases in the atmosphere occurs preferentially at wavelengths in the near-infrared and above, with the exception of ozone which absorbs in the ultraviolet (UV) and visible (VIS) bands. In addition, molecular scattering occurs primarily at the shorter wavelengths in the UV and VIS. Hence, inspired by [35,53,54] proposed a two-band parameterization of the atmospheric transmittances in the CPCR2 clear-sky solar radiation model, which divided the solar spectral band into a UV/VIS band (0.29–0.7 μm) and a infrared (IR) band (0.7–2.7 μm). That approach has been continued in subsequent CSR models [48,49,55] with expanded IR band up to 4 μm.

The E_{bn} parameterization to use in combination with the 2-band independent integration scheme (hereinafter referred to as INDEP-2B) is as follows:

$$\hat{E}_{bn} = E_{on} \sum_{j=1,2} f_j \, T_{oj} T_{rj} T_{gj} T_{wj} T_{aj} \tag{8}$$

where the subscript j refers to the UV/VIS band (j=1) (0.29–0.7 μm) and the IR band (j=2) (0.7–4 μm), respectively, and f_j is the fraction of total extraterrestrial solar irradiance, E_{on}, within each band, such that $f_1 + f_2 = 1$. The broadband transmittances T_{i1} and T_{i2} for the atmospheric constituent i are defined as in Eq. (6) but within the UV/VIS and IR bands, respectively.

2.2. Prescribed interdependent integration scheme

The INTER scheme can be largely simplified to prevent the INTER's pitfall by prescribing the amounts of the atmospheric constituents others than the one that is relevant for each atmospheric transmittance. Assuming a top-down layering of the atmosphere such that the successive transmittance processes are ozone absorption, Rayleigh scattering, molecular absorption, water vapor absorption and extinction by aerosols, the prescribed interdependent broadband transmittances are:

$$T'_o = \frac{\int_{\Delta\lambda} E_{on\lambda} \tau_{o\lambda} d\lambda}{\int_{\Delta\lambda} E_{on\lambda} d\lambda} \tag{9}$$

$$T'_r = \frac{\int_{\Delta\lambda} E_{on\lambda} \tau'_{o\lambda} \tau_{r\lambda} d\lambda}{\int_{\Delta\lambda} E_{on\lambda} \tau'_{o\lambda} d\lambda} \tag{10}$$

$$T'_g = \frac{\int_{\Delta\lambda} E_{on\lambda} \tau'_{o\lambda} \tau'_{r\lambda} \tau_{g\lambda} d\lambda}{\int_{\Delta\lambda} E_{on\lambda} \tau'_{o\lambda} \tau'_{r\lambda} d\lambda} \tag{11}$$

$$T'_w = \frac{\int_{\Delta\lambda} E_{on\lambda} \tau'_{o\lambda} \tau'_{r\lambda} \tau'_{g\lambda} \tau_{w\lambda} d\lambda}{\int_{\Delta\lambda} E_{on\lambda} \tau'_{o\lambda} \tau'_{r\lambda} \tau'_{g\lambda} d\lambda} \tag{12}$$

$$T'_a = \frac{\int_{\Delta\lambda} E_{on\lambda} \tau'_{o\lambda} \tau'_{r\lambda} \tau'_{g\lambda} \tau'_{w\lambda} \tau_{a\lambda} d\lambda}{\int_{\Delta\lambda} E_{on\lambda} \tau'_{o\lambda} \tau'_{r\lambda} \tau'_{g\lambda} \tau'_{w\lambda} d\lambda} \tag{13}$$

where $\tau'_{i\lambda}$ is the spectral transmittance of the *i-th* atmospheric layer calculated for a prescribed amount of the relevant atmospheric constituent, i.e., total-column ozone content for $\tau'_{o\lambda}$, atmospheric pressure for $\tau'_{r\lambda}$ and $\tau'_{g\lambda}$, and precipitable water for $\tau'_{w\lambda}$. This scheme is hereinafter referred to as INTER-P.

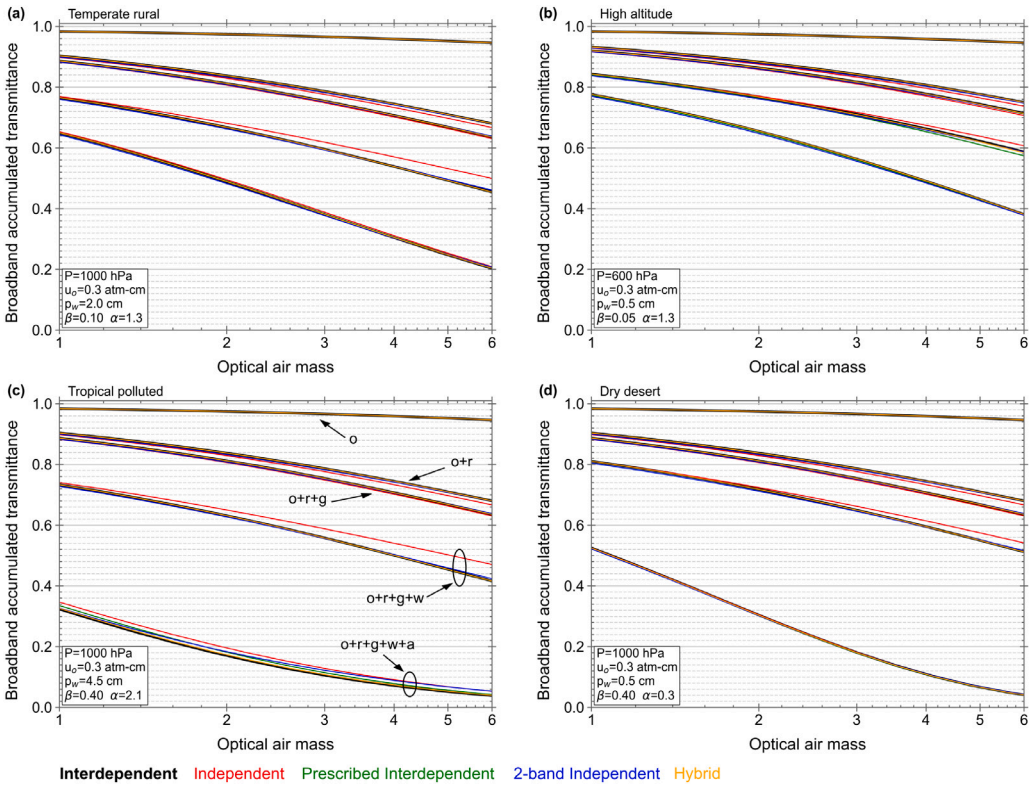

Fig. 1. Cumulative atmospheric broadband transmittance from the top to the bottom layer using the INTER, INDEP, INDEP-2B, INTER-P and HYBRID schemes in four atmospheric environments: (a) temperate rural, (b) high elevation, (c) tropical polluted and (d) dry desert. The top-to-bottom atmospheric transmittances are: ozone absorption, Rayleigh scattering, molecular absorption, water vapor absorption and extinction by aerosols, referred in the lower-left panel to as o, r, g, w and a, respectively.

2.3. Hybrid integration scheme

The INDEP-2B and INTER-P schemes can be combined if E_{bn} is calculated from Eq. (8) and the broadband transmittances are evaluated from Eqs. (9)–(13). This approach is hereinafter referred to as HYBRID scheme.

3. Data and methods

The analysis of the performance of the integration schemes in the evaluation of E_{bn} requires calculating the spectral atmospheric transmittances for all atmospheric constituents, i.e., $\tau_{o\lambda}$, $\tau_{r\lambda}$, $\tau_{g\lambda}$, $\tau_{w\lambda}$ and $\tau_{a\lambda}$, including $\tau'_{o\lambda}$, $\tau'_{r\lambda}$, $\tau'_{g\lambda}$ and $\tau'_{w\lambda}$ with prescribed values of total-column ozone content (0.3 atm-cm), atmospheric pressure (1013 hPa) and precipitable water (1.4 cm). From them, E_{bn} is calculated from Eq. (4) with broadband transmittances successively evaluated using the INDEP and INTER-P schemes, and from Eq. (8), with the INDEP-2B and HYBRID schemes. Last, the results are compared to the true E_{bn} obtained from Eq. (3) to analyze the E_{bn} approximation error in each case. Note that the INTER scheme is not considered here because it is an exact estimator of the true E_{bn}, meaning that its E_{bn} approximation error is always strictly zero. However, this is at the expense of the INTER's pitfall.

In order to generate a comprehensive data set, the former cycle is repeated for all the possible combinations in a selection of values of the most important atmospheric parameters at determining broadband radiation throughout a cloudless atmosphere, namely: thirty log-distributed optical air mass values between 1 and 20 (i.e., solar zenith angle from 0° to about 87°), two values of atmospheric pressure (800 and 1013 hPa), one value of total-column ozone content (0.3 atm-cm), eighty-one equidistant values of precipitable water content between 0 and 5 cm, ninety-seven equidistant values of Ångström's turbidity between 0 and 1.2 and three values of Ångström's exponent (0.3, 1.3 and 2.3). Thus, the transmittance is computed for a total of 1,414,260 hypothetical atmospheres, involving up to 7,071,300 atmospheric spectral transmittances.

To calculate the spectral transmittances by each atmospheric constituent, the SMARTS2 model, version 2.9.5, was initially considered [code publicly available at 56]. This approach, however, was soon deemed unpractical because SMARTS2 requires that the simulation options for every simulated case are provided in an *ascii* file that the model reads in, providing then the simulation results in additional output *ascii* files. Although this is a convenient solution for most of the use cases of the model, in which a reduced number of simulations is aimed, the fact that every simulated case requires writing and reading *ascii* files, makes the process too slow for the purposes of this study.

In addition, since this study only requires the spectral transmittances by individual atmospheric constituents, which represent only a tiny fraction of the total computational burden in SMARTS2, using that model would involve wasting resources in computations that are not needed here. To avoid these shortcomings, the spectral transmittances by each atmospheric constituent have been carefully re-coded in a Python library using the SMARTS2 version 2.9.5 code as a reference. The Python library performs all the calculations in memory, with no need to read/write from/to disk. The code is freely available at https://github.com/jararias/dast/tree/paper, where the scripts to perform all the analyses undertaken here are also provided for public access.

The extraterrestrial solar spectrum used for all the calculations is a recent revised composite spanning the range 0.2–1000 μm, with a focus in the 200–4000 nm waveband, although in this study it is restricted to the 290–4000 nm range. The spectrum and the details of the methods to compose it are provided in [57]. It describes the mean solar spectral irradiance, in W m^{-2} nm^{-1}, at normal incidence and mean Sun–Earth distance in steps of 0.5 nm between 290 and 400 nm, 1 nm between 400 and 1705 nm, and 5 nm between 1705 and 4000 nm, making a total of 1985 wavelengths. The value of E_{on} extended to the entire spectrum is 1361.1 W/m^2.

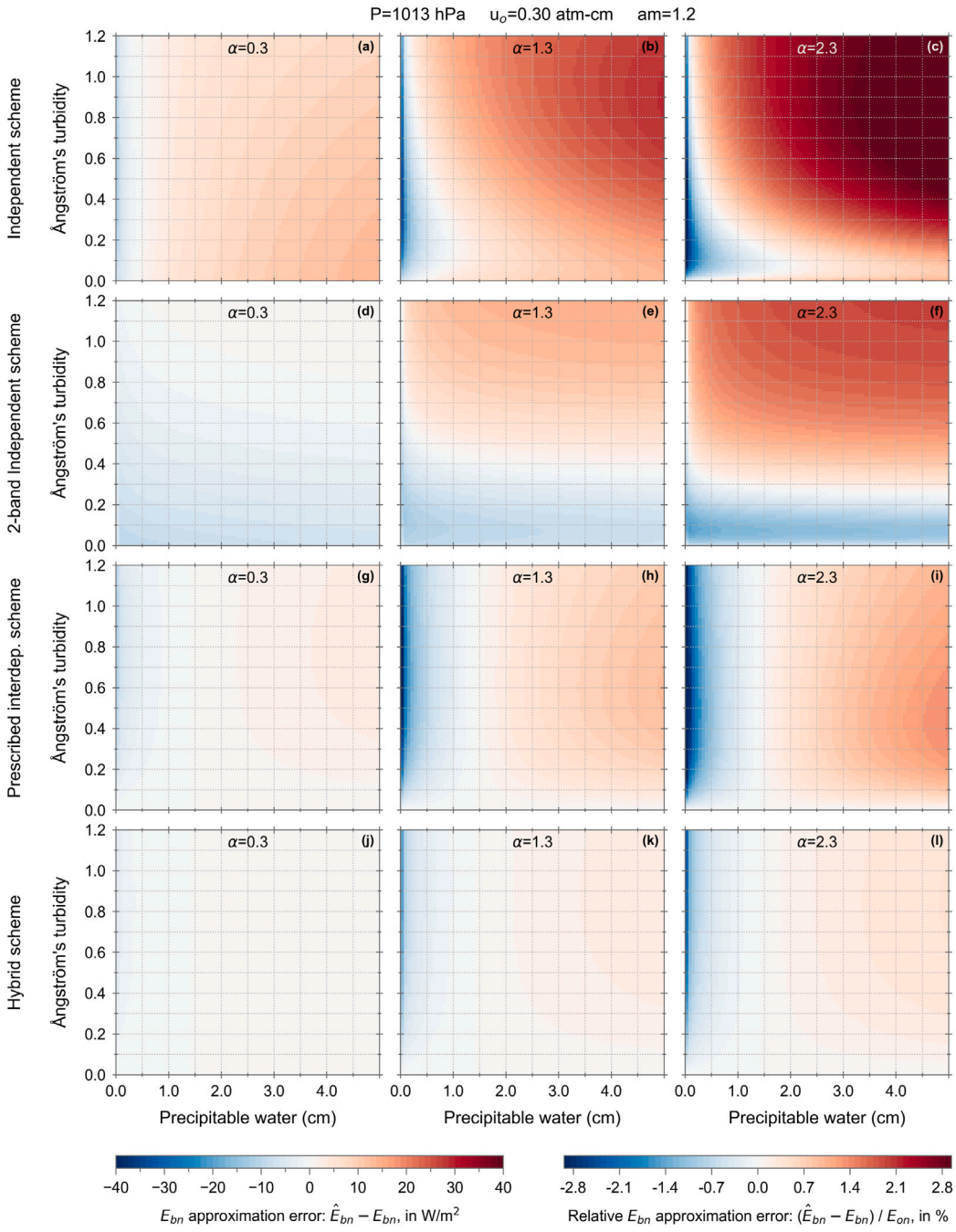

Fig. 2. E_{bn} approximation error using the INDEP, INDEP-2B, INTER-P and HYBRID schemes. The error is presented in the Ångström's turbidity and precipitable water space, for three values of Ångström's exponent (0.3, 1.3 and 2.3). The atmospheric pressure is 1013 hPa, the total-column ozone content is 0.30 atm-cm and air mass is 1.2.

In addition to the nearly 1.5 million hypothetical atmospheres that are simulated, a 1-year hourly worldwide simulation across a 2-degree spatial grid is performed to evaluate the spatial distribution of the E_{bn} approximation errors and disclose regions that might be notably affected by such errors. For the simulation, 1-year of hourly gridded values of total-column ozone content, atmospheric pressure, total-column water vapor content, aerosol optical depth at 550 nm and Ångström's exponent from the NASA's *Modern-Era Retrospective analysis for Research and Applications Version 2* [MERRA-2; 58] are retrieved from [59]. The variables are provided in a 5/8° by 1/2° longitude–latitude grid, and they are linearly interpolated to a 2-degree longitude–latitude grid.

Since Ångström's turbidity is required to evaluate the aerosol spectral transmittance, it is computed from the aerosol optical depth at 550 nm and Ångström's exponent using the Ångström's law [60]. Optical air mass is computed for each atmospheric constituent following the expressions outlined in Appendix A in [3], with solar position evaluated using the PSA's algorithm [61].

4. Results

Inspired by Molineaux and Ineichen [31], Fig. 1 compares the cumulative broadband transmittances as atmospheric layers are successively traversed from the top to the bottom of the atmosphere, for the INTER, INDEP, INDEP-2B, INTER-P and HYBRID schemes in four paradigmatic atmospheres, namely: (a) temperate rural, (b) high elevation, (c) tropical polluted and (d) dry desert. Note that the INTER scheme provides the true E_{bn} so it represents the reference target for the rest of schemes.

In general, after the light has traversed the ozone and molecular layers there is no significant difference in the accumulated broadband transmittances no matter the atmosphere. Nonetheless, after the subsequent water vapor layer the INDEP-based transmittance diverges from the rest, with divergences in the range 2%–6% for air mass greater than about 4 (i.e., solar zenith angles greater than about 70°), more pronounced in the tropical polluted atmosphere and less in the high elevation atmosphere. Interestingly, the errors with the INDEP scheme are compensated in the subsequent aerosol layer in all the atmospheres, meaning that the spectral integration of the aerosol transmittance introduces deviations that are similar in magnitude, but opposed in sign, to the ones existing after the water vapor layer. Only for the tropical polluted atmosphere the differences after the aerosol layer with the INDEP-based transmittances remain significant, staying at about 2% for any solar position. Conversely to the INDEP scheme, the INDEP-2B and INTER-P approaches keep close to the INTER reference scheme, except for the tropical polluted atmosphere in which they may differ up to ≈1%, with the INTER-P slightly better than INDEP-2B. Only the HYBRID scheme is able to match the INTER reference under all circumstances.

These results suggest that there are environmental conditions that enhance the errors of the INDEP scheme, such as in clean and humid atmospheres. This would be the situation, for instance, in the temperate rural and tropical polluted cases if the aerosol load was low. Under these conditions, it is expected that the E_{bn} predictions by models built on the INDEP scheme produce biased results.

In order to explore in depth all possible situations, and not only the ones presented in Fig. 1, Fig. 2 shows the E_{bn} parameterization error for air mass 1.2 using the INDEP, INDEP-2B, INTER-P and HYBRID schemes in the Ångström's turbidity–precipitable water space, for three values of Ångström's exponent: 0.3 (coarse aerosol, typical in situations dominated by dust or sea salt), 1.3 (mixed aerosol, typical in rural or continental conditions) and 2.3 (fine aerosol, typical in situations dominated by anthropogenic pollution) [62,63]. The INDEP scheme always overestimates the true E_{bn} except for very dry conditions. The overall error increases with growing precipitable water, Ångström's turbidity and Ångström's exponent, becoming eventually larger than 40 W/m^2 in humid polluted conditions (or, equivalently, larger than 3% of E_{on}, where E_{on} is taken as 1361.1 W/m^2). When E_{bn} is evaluated using the INDEP-2B scheme, the overall error diminishes noticeably. It even virtually vanishes when Ångström's exponent is 0.3, but increases for greater Ångström's exponents. Overall, the error barely depends on precipitable water, but it does on Ångström's turbidity. In particular, it underestimates the E_{bn} values under clean atmospheres, and overestimates under turbid situations, even reaching ≈25 W/m^2 in extremely polluted situations (or, equivalently, ≈2% of E_{on}).

The INTER-P scheme further reduces the difference with respect to the true E_{bn}, which is not greater than about 1.5% of E_{on} under any circumstance. Nonetheless, this scheme yields a detrimental underestimation of E_{bn} under dry and very dry conditions that turns into overestimation with humid situations. The error now grows with increasing precipitable water, but barely depends on Ångström's turbidity. As with the INDEP-2B scheme, the error slightly increases with Ångström's exponent.

The HYBRID scheme shows an outstanding performance. As expected, it combines features of both the INDEP-2B and INTER-P schemes: its error barely depends on precipitable water, as with the INDEP-2B, and barely depends on Ångström's turbidity, as with the INTER-P scheme. However, it keeps some residual underestimation for extremely dry atmospheres, likely inherited from the INTER-P scheme. The existing dependency on Ångström's exponent in the INDEP-2B and INTER-P schemes is barely noticeable here. The difference with respect to the true E_{bn} is nearly always bounded within the approximated range ±5 W/m^2 or, equivalently, ±0.4% of E_{on}.

When Fig. 2 is replicated for air mass 3 (not shown here) the error and its pattern stay roughly the same as for air mass 1.2, except for the INDEP scheme, for which the error grows significantly under clean conditions.

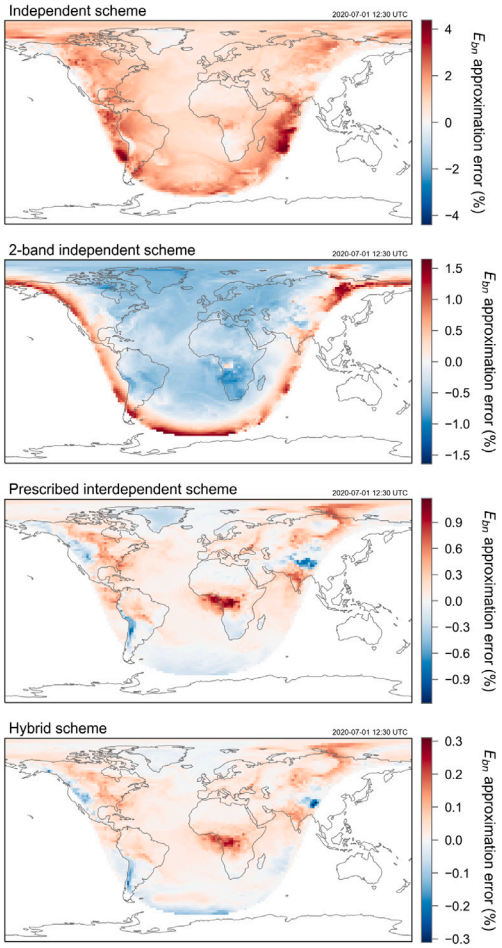

Fig. 3. Worldwide relative E_{bn} approximation error, in % of E_{on}, on 2020-07-01 at 12:30 UTC, using the INDEP, INDEP-2B, INTER-P and HYBRID schemes. The error is evaluated as $\left(\hat{E}_{bn} - E_{bn}\right)/E_{on}$. Note the different color scales.

4.1. Worldwide evaluation

The comparison shown in Figs. 1 and 2 depicts only a partial view of the impact of the broadband transmittance integration scheme as it does not account for the particular weather patterns at the location of interest. To that aim, the 1-year hourly worldwide simulation described in Section 3 is performed.

Fig. 3, which shows the E_{bn} approximation error on 2020-07-01 at 12:30 UTC for illustration purposes, reveals interesting spatial error patterns, such as the generalized worldwide overestimation with the INDEP scheme, by about 1% on average, and with peaks above 4%, in contrast with the general underestimation with the INDEP-2B scheme by about −0.5% on average, except for high air mass, where the scheme overestimates by about 0.5% on average, but with peaks above 1.5%, specially in expectedly clean situations. The INTER-P scheme solves the INDEP-2B's issue at high air masses and results in lower overall errors than the previous schemes, to the point that 90% of the errors are within ±0.3%. In correspondence with the results shown in Fig. 2, INTER-P underestimates in dry regions such as in high mountains, arid regions, and Greenland, and it overestimates in expectedly wet regions, such as, areas in the Equatorial belt. The HYBRID scheme yields similar spatial patterns to those of the INTER-P scheme, but with lower overall error (90% of the errors are within ±0.07%).

In order to analyze the typical spatial error patterns, Fig. 4 shows the mean relative error throughout the entire 1-year simulation described in Section 3. As it was anticipated in Fig. 3, the INDEP and

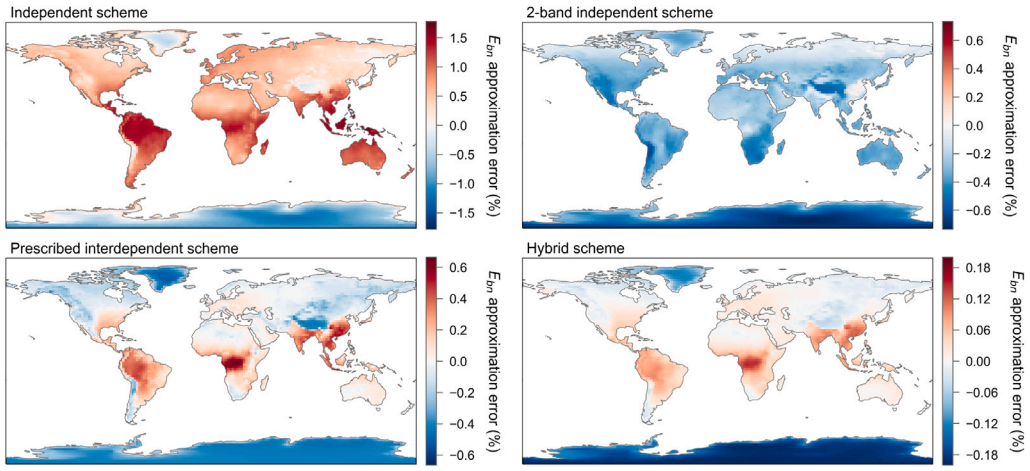

Fig. 4. Worldwide mean relative E_{bn} approximation error, in % of E_{on}, using the INDEP, INDEP-2B, INTER-P and HYBRID schemes. The error is evaluated as $\left(\hat{E}_{bn} - E_{bn}\right)/E_{on}$. Note the different color scales.

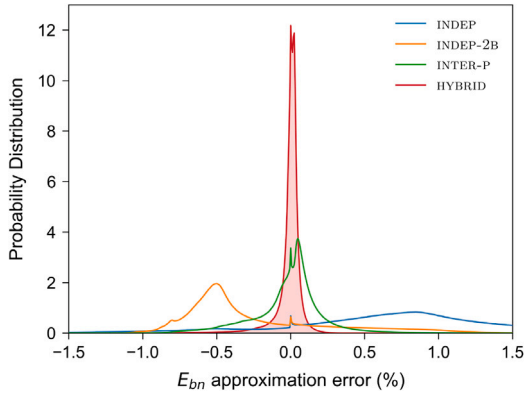

Fig. 5. Probability distribution of the relative E_{bn} approximation error, in % of E_{on} for the INDEP, INDEP-2B, INTER-P and HYBRID schemes. The error is evaluated as $\left(\hat{E}_{bn} - E_{bn}\right)/E_{on}$.

INDEP-2B schemes result in overall overestimation and underestimation, respectively, of the true E_{bn}. Now, however, it is apparent that INDEP also underestimates in very dry areas such as Greenland, the Himalayas and Antarctica. The spatial error patterns for the INTER-P and HYBRID schemes are very similar to those already described in Fig. 3. In essence, both schemes underestimate in dry and mostly clean regions (Greenland, Northwest America, Andes, the Himalayas, Russia and Antarctica) and overestimate in humid polluted regions, mostly in the Equatorial belt area, Southern Asia, Southeastern America and slightly in Europe. Of interest, however, is the successive error reduction from the INDEP scheme through the HYBRID scheme. While 90% of the average errors in the former are bounded within ±1.4% of E_{on}, the HYBRID scheme keeps 90% of its average errors within ±0.1%. For the INDEP-2B and INTER-P schemes, they are bounded within ±0.4%. This trend is also observed in the probability distributions of the worldwide hourly errors for each integration scheme, which is shown in Fig. 5.

5. Conclusions

Broadband atmospheric transmittances are key components of many broadband clear-sky solar radiation models that are routinely used worldwide in solar applications. These transmittances are built after a two-step process in which, first, the spectral atmospheric transmittance is integrated, and, second, the integrated transmittances are parameterized as custom functions of solar position and atmospheric state. Then, the broadband transmittances are combined in a model to compute direct normal irradiance. This work analyzes the contribution of the assumptions made in the integration step to the final model error at approximating the true direct normal irradiance.

Typically, two spectral integration schemes, INDEP and INTER, have been considered in the topical scientific literature. In practice, however, the INDEP scheme is the one used virtually always, arguably because it simplifies the subsequent parameterization step, despite it also introduces a far from negligible error in many situations, as it is here demonstrated. For instance, such error can be as high as ±40 W/m^2 in dry and clean, and in humid and turbid conditions, which are frequent in many areas worldwide.

This work proposes various alternative versions of the INDEP and INTER integration schemes that largely mitigate the issues typically associated with the INDEP's pitfall and the INTER's pitfall. The study conducted here evaluates for the first time, and at worldwide scale, the expected approximation error of direct normal irradiance which is directly attributable to the choice of spectral integration scheme of the atmospheric transmittances. It is shown that such error stays within ±1.5 W/m^2 for 90% of the cases found in a 1-year hourly simulation conducted worldwide using data from the NASA's MERRA2 atmospheric reanalysis when the here proposed HYBRID integration scheme is used. Conversely, using the ubiquitous INDEP integration scheme, the error that encompasses 90% of the cases climbs up to about ±20 W/m^2, but can be eventually much higher.

It is concluded that a broadband clear-sky solar radiation model devised to be used worldwide must necessarily reject the INDEP integration scheme and consider an alternative approach, tentatively, one of the alternatives proposed here.

Declaration of competing interest

The authors declare that they have no known competing financial interests or personal relationships that could have appeared to influence the work reported in this paper.

References

[1] Iqbal Muhammad. An introduction to solar radiation. Academic Press; 1983.
[2] Bohren CF, Clothiaux EE. Fundamentals of Atmospheric Radiation: An Introduction with 400 Problems. Weinheim, Germany: Wiley–CH; 2006.
[3] Gueymard CA. Parameterized transmittance model for direct beam and circumsolar spectral irradiance. Sol Energy 2001;71(5):325–46. http://dx.doi.org/10.1016/S0038-092X(01)00054-8.
[4] Gueymard CA. Direct solar transmittance and irradiance predictions with broadband models. Part I: detailed theoretical performance assessment. Sol Energy 2003;74(5):355–79. http://dx.doi.org/10.1016/S0038-092X(03)00195-6.
[5] Myers Daryl R. Solar Radiation: Practical Modeling for Renewable Energy Applications. Boca Raton, FL: CRC Press; 2013.

[6] Sengupta Manajit, Habte Aron, Wilbert Stefan, Gueymard Christian, Remund Jan. Best Practices Handbook for the Collection and Use of Solar Resource Data for Solar Energy Applications: Third Edition. Tech. Rep. NREL/TP-5D00-77635, Golden, CO: National Renewable Energy Laboratory; 2021.
[7] Long CN, Shi Y. An automated quality assessment and control algorithm for surface radiation measurements. J Open Atmos Sci 2008;2:23–37. http://dx.doi.org/10.2174/1874282300802010023.
[8] Gueymard Christian A. Clear-sky irradiance predictions for solar resource mapping and large-scale applications: Improved validation methodology and detailed performance analysis of 18 broadband radiative models. Sol Energy 2012;86(8):2145–69. http://dx.doi.org/10.1016/j.solener.2011.11.011.
[9] Perez Richard, Cebecauer Tomás, Šúri Marcel. Semi-empirical satellite models. In: Kleissl Jan, editor. Solar Energy Forecasting and Resource Assessment. Elsevier; 2013, p. 21–48. http://dx.doi.org/10.1016/B978-0-12-397177-7.00002-4.
[10] Engerer NA, Mills FP. KPV: A Clear-sky index for photovoltaics. Sol Energy 2014;105:679–93. http://dx.doi.org/10.1016/j.solener.2014.04.019.
[11] Bright JM, Smith CJ, Taylor PG, Crook R. Stochastic generation of synthetic minutely irradiance time series derived from mean hourly weather observation data. Sol Energy 2015;115:229–42. http://dx.doi.org/10.1016/j.solener.2015.02.032.
[12] Ruiz-Arias José A, Gueymard Christian A. Solar resource for high-concentrator photovoltaic applications. In: Pérez-Higueras Pedro, Fernández Eduardo F, editors. High Concentrator Photovoltaics: Fundamentals, Engineering and Power Plants. 2015, p. 261–302. http://dx.doi.org/10.1007/978-3-319-15039-0_10.
[13] Gueymard Christian A. Clear-sky radiation models and aerosol effects. In: Polo Jesús, Martín-Pomares Luis, Sanfilippo Antonio, editors. Solar Resources Mapping. Springer International Publishing; 2019, p. 137–82. http://dx.doi.org/10.1007/978-3-319-97484-2{_}5.
[14] Ruiz-Arias José A, Gueymard Christian A, Cebecauer Tomas. Direct normal irradiance modeling: Evaluating the impact on accuracy of worldwide gridded aerosol databases. AIP Conf Proc 2019;2126(1):190013. http://dx.doi.org/10.1063/1.5117710.
[15] Polo Jesús, Perez Richard. Solar radiation modeling from satellite imagery. In: Polo Jesús, Martín-Pomares Luis, Sanfilippo Antonio, editors. Solar Resources Mapping: Fundamentals and Applications. Springer; 2019, p. 183–97. http://dx.doi.org/10.1007/978-3-319-97484-2_6.
[16] Gueymard Christian A, Bright Jamie M, Lingfors David, Habte Aron, Sengupta Manajit. A posteriori clear-sky identification methods in solar irradiance time series: review and preliminary validation using sky imagers. Renew Sust Energ Rev 2019;109:412–27. http://dx.doi.org/10.1016/j.rser.2019.04.027.
[17] Liu Hongda, Li Lun, Han Yang, Lu Fang. Method of identifying the lengths of equivalent clear-sky periods in the time series of DNI measurements based on generalized atmospheric turbidity. Renew Energ 2019;136:179–92. http://dx.doi.org/10.1016/j.renene.2018.12.119.
[18] Munkhammar Joakim, van der Meer Dennis, Widén Joakim. Probabilistic forecasting of high-resolution clear-sky index time-series using a Markov-chain mixture distribution model. Sol Energy 2019;184:688–95. http://dx.doi.org/10.1016/j.solener.2019.04.014.
[19] van der Meer Dennis, Yang Dazhi, Widén Joakim, Munkhammar Joakim. Clear-sky index space-time trajectories from probabilistic solar forecasts: Comparing promising copulas. J Renew Sust Energ 2020;12(2):026102. http://dx.doi.org/10.1063/1.5140604.
[20] Badescu Viorel, Gueymard Christian A, Cheval Sorin, Oprea Cristian, Baciu Madalina, Dumitrescu Alexandru, Iacobescu Flavius, Milos Ioan, Rada Costel. Computing global and diffuse solar hourly irradiation on clear sky. Review and testing of 54 models. Renew Sust Energ Rev 2012;16(3):1636–56. http://dx.doi.org/10.1016/j.rser.2011.12.010.
[21] Reno Matthew J, Hansen Clifford W, Stein Joshua S. Global Horizontal Irradiance Clear Sky Models: Implementation and Analysis. Tech. Rep. SAND2012-2389, Albuquerque, NM: Sandia National Laboratories; 2012, http://dx.doi.org/10.2172/1039404.
[22] Gueymard Christian A, Ruiz-Arias José Antonio. Validation of direct normal irradiance predictions under arid conditions: A review of radiative models and their turbidity-dependent performance. Renew Sust Energ Rev 2015;45:379–96. http://dx.doi.org/10.1016/j.rser.2015.01.065.
[23] Ruiz-Arias José A, Gueymard Christian A. Worldwide inter-comparison of clear-sky solar radiation models: Consensus-based review of direct and global irradiance components simulated at the earth surface. Sol Energy 2018;168:10–29. http://dx.doi.org/10.1016/j.solener.2018.02.008.
[24] Ruiz-Arias José A, Gueymard Christian A. A multi-model benchmarking of direct and global clear-sky solar irradiance predictions at arid sites using a reference physical radiative transfer model. Sol Energy 2018;171:447–65. http://dx.doi.org/10.1016/j.solener.2018.06.048.
[25] Antonanzas-Torres F, Urraca R, Polo J, Perpiñán Lamigueiro O, Escobar R. Clear sky solar irradiance models: A review of seventy models. Renew Sust Energ Rev 2019;107:374–87. http://dx.doi.org/10.1016/j.rser.2019.02.032.
[26] Sun Xixi, Bright Jamie M, Gueymard Christian A, Acord Brendan, Wang Peng, Engerer Nicholas A. Worldwide performance assessment of 75 global clear-sky irradiance models using Principal Component Analysis. Renew Sust Energ Rev 2019;111:550–70. http://dx.doi.org/10.1016/j.rser.2019.04.006.
[27] Sun Xixi, Bright Jamie M, Gueymard Christian A, Bai Xinyu, Acord Brendan, Wang Peng. Worldwide performance assessment of 95 direct and diffuse clear-sky irradiance models using principal component analysis. Renew Sust Energ Rev 2021;135:110087. http://dx.doi.org/10.1016/j.rser.2020.110087.
[28] Liou Kuo-Nan. An introduction to atmospheric radiation. vol. 84, Elsevier; 2002.
[29] van de Hulst Hendrik Christoffel. Light scattering by small particles. New York: Dover Publications; 1981.
[30] Bird RE, Hulstrom RL. Simplified clear sky model for direct and diffuse insolation on horizontal surfaces. Tech. Rep. SERI/TR-642-761, Golden, CO: Solar Energy Research Institute; 1981, http://dx.doi.org/10.2172/6510849.
[31] Molineaux Benoît, Ineichen Pierre. On the broad band transmittance of direct irradiance in a cloudless sky and its application to the parameterization of atmospheric turbidity. Sol Energy 1996;56(6):553–63. http://dx.doi.org/10.1016/0038-092X(96)00016-3.
[32] Gueymard CA. Multilayer-weighted transmittance functions for use in broadband irradiance and turbidity calculations. American Solar Energy Society, Boulder, CO; 1996.
[33] Gueymard Christian A. Turbidity determination from broadband irradiance measurements: A detailed multicoefficient approach. J Appl Meteorol 1998;37(4):414–35. http://dx.doi.org/10.1175/1520-0450(1998)037<0414:TDFBIM>2.0.CO;2.
[34] Gueymard Christian. An atmospheric transmittance model for the calculation of the clear sky beam, diffuse and global photosynthetically active radiation. Agr Forest Meteorol 1989;45(3):215–29. http://dx.doi.org/10.1016/0168-1923(89)90045-2.
[35] Gueymard CA. A two-band model for the calculation of clear sky solar irradiance, illuminance, and photosynthetically active radiation at the earth's surface. Sol Energy 1989;43(5):253–65. http://dx.doi.org/10.1016/0038-092X(89)90113-8.
[36] Psiloglou BE, Santamouris M, Asimakopoulos DN. On the atmospheric water vapor transmission function for solar radiation models. Sol Energy 1994;53(5):445–53. http://dx.doi.org/10.1016/0038-092X(94)90059-0.
[37] Psiloglou BE, Santamouris M, Asimakopoulos DN. Predicting the broadband transmittance of the uniformly mixed gases (CO2, CO, N2O, CH4 and O2) in the atmosphere, for solar radiation models. Renew Energ 1995;6(1):63–70. http://dx.doi.org/10.1016/0960-1481(94)00062-B.
[38] Psiloglou BE, Santamouris M, Asimakopoulos DN. On broadband Rayleigh scattering in the atmosphere for solar radiation modelling. Renew Energ 1995;6(4):429–33. http://dx.doi.org/10.1016/0960-1481(94)00084-J.
[39] Psiloglou BE, Santamouris M, Varotsos C, Asimakopoulos DN. A new parameterization of the integral ozone transmission. Sol Energy 1996;56(6):573–81. http://dx.doi.org/10.1016/0038-092X(96)00030-8.
[40] Psiloglou BE, Santamouris M, Asimakopoulos DN. Predicting the spectral and broadband aerosol transmittance in the atmosphere for solar radiation modelling. Renew Energ 1997;12(3):259–79. http://dx.doi.org/10.1016/S0960-1481(97)00044-X.
[41] Psiloglou BE, Santamouris M, Asimakopoulos DN. Atmospheric broadband model for computation of solar radiation at the Earth's surface. Application to mediterranean climate. Pure Appl. Geophys. 2000;157:829–60. http://dx.doi.org/10.1007/PL00001120.
[42] Yang K, Huang GW, Tamai N. A hybrid model for estimating global solar radiation. Sol Energy 2001;70(1):13–22. http://dx.doi.org/10.1016/S0038-092X(00)00121-3.
[43] Yang Kun, Koike Toshio, Ye Baisheng. Improving estimation of hourly, daily, and monthly solar radiation by importing global data sets. Agricult Forest Meterol 2006;137(1-2):43–55. http://dx.doi.org/10.1016/j.agrformet.2006.02.001.
[44] Calinoiu Delia, Paulescu Marius, Ionel Ioana, Stefu Nicoleta, Pop Nicolina, Boata Remus, Pacurar Angel, Gravila Paul, Paulescu Eugenia, Trif-Tordai Gavrila. Influence of aerosols pollution on the amount of collectable solar energy. Energ Convers Manage 2013;70:76–82. http://dx.doi.org/10.1016/j.enconman.2013.02.012.
[45] Kambezidis HD, Psiloglou BE, Karagiannis D, Dumka UC, Kaskaoutis DG. Recent improvements of the meteorological radiation model for solar irradiance estimates under all-sky conditions. Renew Energ 2016;93:142–58. http://dx.doi.org/10.1016/j.renene.2016.02.060.
[46] Calinoiu Delia, Stefu Nicoleta, Boata Remus, Blaga Robert, Pop Nicolina, Paulescu Eugenia, Sabadus Andreea, Paulescu Marius. Parametric modeling: A simple and versatile route to solar irradiance. Energ Convers Manage 2018;164:175–87. http://dx.doi.org/10.1016/j.enconman.2018.02.077.
[47] Paulescu Eugenia, Paulescu Marius. A new clear sky solar irradiance model. Renew Energ 2021;179:2094–103. http://dx.doi.org/10.1016/j.renene.2021.08.029.
[48] Ruiz-Arias José A. Aerosol transmittance for clear-sky solar irradiance models: Review and validation of an accurate universal parameterization. Renew Sust Energ Rev 2021;145:111061. http://dx.doi.org/10.1016/j.rser.2021.111061.
[49] Gueymard CA. REST2: High-performance Solar radiation model for cloudless-sky irradiance, illuminance, and photosynthetically active radiation–Validation with a benchmark dataset. Sol Energy 2008;82(3):272–85. http://dx.doi.org/10.1016/j.solener.2007.04.008.

[50] Gueymard C. SMARTS2: A Simple Model of the Atmospheric Radiative Transfer of Sunshine: Algorithms and performance assessment. Tech. Rep. FSEC-PF-270-95, Cocoa, FL: Florida Solar Energy Center / University of Central Florida; 1995, http://www.fsec.ucf.edu/en/publications/pdf/FSEC-PF-270-95.pdf.

[51] Gueymard Christian A. Interdisciplinary applications of a versatile spectral solar irradiance model: A review. Energy 2005;30(9):1551–76. http://dx.doi.org/10.1016/j.energy.2004.04.032.

[52] Gueymard Christian A. The SMARTS spectral irradiance model after 25 years: New developments and validation of reference spectra. Sol Energy 2019;187:233–53. http://dx.doi.org/10.1016/j.solener.2019.05.048.

[53] Lacis Andrew, Hansen James. A parameterization for the absorption of solar radiation in the Earth's atmosphere. J Atmos Sci 1974;31(1):118–33. http://dx.doi.org/10.1175/1520-0469(1974)031<0118:APFTAO>2.0.CO;2.

[54] Paulin Gaston. Simulation de l'énergie solaire au sol. Atmosphere-Ocean 1980;18(4):286–303. http://dx.doi.org/10.1080/07055900.1980.9649093.

[55] Sun Zhian, Liu Aixia. Fast scheme for estimation of instantaneous direct solar irradiance at the Earth's surface. Sol Energy 2013;98:125–37. http://dx.doi.org/10.1016/j.solener.2012.12.013.

[56] NREL. National Renewable Energy Laboratory. 2021, https://www.nrel.gov/grid/solar-resource/smarts.html.

[57] Gueymard Christian A. Revised composite extraterrestrial spectrum based on recent solar irradiance observations. Sol Energy 2018;169:434–40. http://dx.doi.org/10.1016/j.solener.2018.04.067.

[58] Gelaro Ronald, McCarty Will, Suárez Max J, Todling Ricardo, Molod Andrea, Takacs Lawrence, Randles Cynthia A, Darmenov Anton, Bosilovich Michael G, Reichle Rolf, Wargan Krzysztof, Coy Lawrence, Cullather Richard, Draper Clara, Akella Santha, Buchard Virginie, Conaty Austin, da Silva Arlindo M, Gu Wei, Kim Gi-Kong, Koster Randal, Lucchesi Robert, Merkova Dagmar, Nielsen Jon Eric, Partyka Gary, Pawson Steven, Putman William, Rienecker Michele, Schubert Siegfried D, Sienkiewicz Meta, Zhao Bin. The modern-era retrospective analysis for research and applications, version 2 (MERRA-2). J Climate 2017;30(14):5419–54. http://dx.doi.org/10.1175/JCLI-D-16-0758.1.

[59] GMAO. Global Modeling and Assimilation Office, Goddard Space Flight Center, NASA. 2021, https://gmao.gsfc.nasa.gov/reanalysis/MERRA-2/.

[60] Ångström Anders. On the atmospheric transmission of sun radiation and on dust in the air. Geogr Ann 1929;11:156–66. http://dx.doi.org/10.2307/519399.

[61] Blanco Manuel J, Milidonis Kypros, Bonanos Aristices M. Updating the PSA sun position algorithm. Sol Energy 2020;212:339–41. http://dx.doi.org/10.1016/j.solener.2020.10.084.

[62] Ruiz-Arias José A, Gueymard Christian A, Quesada-Ruiz Samuel, Santos-Alamillos Francisco J, Pozo-Vázquez David. Bias induced by the AOD representation time scale in long-term solar radiation calculations. Part 1: Sensitivity of the AOD distribution to the representation time scale. Sol Energy 2016;137:608–20. http://dx.doi.org/10.1016/j.solener.2016.06.026.

[63] Ruiz-Arias José A, Gueymard Christian A, Santos-Alamillos Francisco J, Quesada-Ruiz Samuel, Pozo-Vázquez David. Bias induced by the AOD representation time scale in long-term solar radiation calculations. Part 2: Impact on long-term solar irradiance predictions. Sol Energy 2016;135:625–32. http://dx.doi.org/10.1016/j.solener.2016.06.017.